EXTENDED EXPERIMENTAL PROCEDURES

Yeast Strains and Growth Conditions

Yeast strains used in this study are listed in Table S1.

Standard media and growth conditions were used for plasmid and yeast genetic manipulations. The *rsr1::HIS3* (Schenkman et al., 2002) and *rsr1::TRP1* (Howell et al., 2009) disruptions were previously described. *cdc42::TRP1* was generated by the one step PCR-based method (Baudin et al., 1993) using ASH58 and ASH59 primers and pRS304 (Sikorski and Hieter, 1989) as template.

Strains containing *BEM1-GFP* (Kozubowski et al., 2008), *CDC3-mCherry* (Howell et al., 2009), and *ABP1-mCherry* (Howell et al., 2009) at the corresponding endogenous loci were generated as previously described. *CDC24-GFP*, *BEM1-tdTomato*, and *PBD-tdTomato* were generated using the PCR-based C-terminal tagging method (Longtine et al., 1998). The *CDC24-GFP* PCR primers (CFW1 and CFW3) were designed to create a linker (CTCGAGCTC) between Cdc24p and GFP, and pDLB51 (*pFA6a-GFP-ADH1t-TRP1*) was used as a template. *BEM1-tdTomato* was created using oligos Z588 and Z589 and pDLB3299 (*pFA6a-tdTomato-ADH1t-HIS3MX6*) as template. *PBD-tdTomato* at the *GIC2* locus was generated by inserting the *tdTomato* sequence after *GIC2* nucleotide 624, which creates a truncation of *GIC2* after the Cdc42p-interacting domain fused to *tdTomato*. Primers Z679 and Z680 were used with template pDLB3301 (*pFA6a-tdTomato-ADH1t-kanMX6*) to amplify the *tdTomato* sequence for integration at *GIC2*. Strains containing *GFP-CDC42* were generated by cutting pDLB3457 (*Yip211-P_{CDC42}-GFP-CDC42*) (Bi et al., 2000) at the unique *EcoRV* site to integrate *GFP-CDC42* at the *URA3* locus. Strains containing *myc-GFP-CDC42* were generated by cutting pDLB3261 (*pRS306-P_{CDC42}-MG-CDC42*) (Wedlich-Soldner et al., 2003) at the unique *EcoRV* site to integrate *myc-GFP-CDC42* at the *URA3* locus.

Strains overexpressing *CDC42* were constructed by replacing P_{CDC42} with P_{GAL1} using the PCR-based method (Longtine et al., 1998). Primers CFW4 and CFW5 were used with template pDLB2316 (*pFA6a-kanMX6-P_{GAL1}*). Strains overexpressing *CDC24* were constructed by replacing P_{CDC24} with P_{GAL1}using primers ASH35 and ASH36 and template pDLB2318 (*pFA6a-His3MX6-P_{GAL1}*). C-terminal HA-tagging of *CDC24* was done using primers CFW1 and CFW3 and template pDLB2307 (*pFA6a-3HA-kanMX6*). P_{GAL1}-dependent expression of *CDC42* or *CDC24-HA* in response to β-estradiol was achieved by integration of the synthetic transcription factor *GAL4DBD-hER-VP16* at *URA3* as previously described (Howell et al., 2009; Takahashi and Pryciak, 2008). Strains overexpressing *CDC24-GFP-CLA4* were constructed by integrating BamHI-linearized DLB3605 plasmid [*pRS305-P_{GAL1}-CDC24(ΔPB1)-GFP-CLA4(nt 4-1292)*] at *CLA4* locus.

Oligonucleotides

Oligonucleotides are listed in Table S2.

Western Blotting

For Western blot analysis, 10^7 cells were collected and total protein was extracted by TCA precipitation as described (Keaton et al., 2008). Electrophoresis and Western blotting were performed as described (Bose et al., 2001). Monoclonal mouse anti-Cdc42p antibodies (Wu and Brennwald, 2010) were used at 1:500 dilution. Monoclonal mouse anti-HA antibody (Roche Applied Science) was used at a 1:2000 dilution. Polyclonal rabbit anti-Cdc11p antibody (Santa Cruz Biotechnology) was used at a 1:5000 dilution. Fluorophore-conjugated secondary antibodies against mouse (IRDye800 conjugated anti-mouse IgG, Rockland Immunochemicals) or rabbit (Alexa Fluor 680 goat anti-rabbit IgG, Invitrogen) antibodies were used at 1:5000 dilution. Blots were visualized by ODYSSEY imaging system (LI-COR Biosciences).

Mathematical Modeling

Modeling Oscillatory Polarization with Negative Feedback

(1) *Positive feedback only.* This model is similar to the one developed by Goryachev (Goryachev and Pokhilko, 2008; Howell et al., 2009), with the simplifying assumption that the role of the GDI, which binds GDP-Cdc42p and allows it to exchange between membrane and cytoplasm (Johnson et al., 2009), can be incorporated in the rate constants for GDP-Cdc42p exchange between membrane and cytoplasm (Figure S3). Other model assumptions include:

(i) GDP-Cdc42p can exchange between the plasma membrane and cytoplasm. The membrane-bound and cytoplasmic forms are labeled as Cdc42D and $\underline{\text{Cdc42l}}_c$, respectively. GTP-Cdc42p (Cdc42T) is always associated with the plasma membrane.

(ii) The Bem1p complex can exchange between cytoplasm (indicated as Bem1GEF_c) and membrane (indicated as Bem1GEF_m). Either form can bind to GTP-Cdc42p on the membrane, generating a complex indicated as Bem1GEFCdc42T.

(iii) The GEF activity of the Bem1p complex increases 2-fold when it binds GTP-Cdc42p (Howell et al., 2009).

(iv) GAP activity is spatially uniform and is incorporated in the first-order hydrolysis rate constant k_{2r}.

(v) The GEF and GAP are not saturated by substrate (GDP-Cdc42p or GTP-Cdc42p respectively).

(vi) The cell dimensions, total Cdc42p, and total Bem1p complex are all constant. The ratio of membrane volume to cytoplasmic volume is indicated by η.

(vii) All membrane-bound species have the same diffusion coefficient, D_m, and all cytosolic species the same diffusion coefficient, D_c, with $D_c >> D_m$.

Model parameter values are listed in Table S3 below. This model is described by the following reaction-diffusion equations:

$$\frac{\partial Cdc42I_c}{\partial t} = D_c\nabla^2 Cdc42I_c + \eta(-k_1 Cdc42I_c + k_{1r} Cdc42D)$$

$$\frac{\partial Cdc42D}{\partial t} = D_m\nabla^2 Cdc42D + k_1 Cdc42I_c - k_{1r} Cdc42D - Cdc42D(k_2 Bem1GEF_m + k_{2p} Bem1GEFCdc42T) + k_{2r} Cdc42T$$

$$\frac{\partial Cdc42T}{\partial t} = D_m\nabla^2 Cdc42T + Cdc42D(k_2 Bem1GEF_m + k_{2p} Bem1GEFCdc42T) - k_{2r} Cdc42T - (k_4 Bem1GEF_c + k_5 Bem1GEF_m) Cdc42T + k_{5r} Bem1GEFCdc42T$$

$$\frac{\partial Bem1GEFCdc42T}{\partial t} = D_m\nabla^2 Bem1GEFCdc42T + (k_4 Bem1GEF_c + k_5 Bem1GEF_m) Cdc42T - k_{5r} Bem1GEFCdc42T$$

$$\frac{\partial Bem1GEF_c}{\partial t} = D_c\nabla^2 Bem1GEF_c + \eta(-k_3 Bem1GEF_c + k_{3r} Bem1GEF_m - k_4 Bem1GEF_c \cdot Cdc42T)$$

$$\frac{\partial Bem1GEF_m}{\partial t} = D_m\nabla^2 Bem1GEF_m + k_3 Bem1GEF_c - k_{3r} Bem1GEF_m - k_5 Bem1GEF_m \cdot Cdc42T + k_{5r} Bem1GEFCdc42T$$

(2) *Negative feedback via GAP activation.* We assume that GTP-Cdc42p activates a cytoplasmic GAP, perhaps by phosphorylation of the GAP by the PAK Cla4p (Cla4p is a Cdc42p effector and part of the Bem1p complex) (Figure S3). The total GAP concentration is assumed to be 1 μM. The two states of the GAP are denoted as GAP_c (basal GAP activity) and GAP^*_c (high GAP activity). Active GAP is γ-fold more active than basal GAP. We imagine that a PAK bound to one molecule of GTP-Cdc42p would phosphorylate a GAP molecule transiently bound to a neighboring molecule of GTP-Cdc42p, so the GAP activation rate would be proportional to the product Bem1GEFCdc42T x Cdc42T x GAP_c. GAP inactivation is assumed to occur in the cytoplasm at a constant rate k_7. Model parameter values are listed in Table S3 below. This model is described by the following equations:

$$\frac{\partial Cdc42I_c}{\partial t} = D_c\nabla^2 Cdc42I_c + \eta(-k_1 Cdc42I_c + k_{1r} Cdc42D)$$

$$\frac{\partial Cdc42D}{\partial t} = D_m\nabla^2 Cdc42D + k_1 Cdc42I_c - k_{1r} Cdc42D - Cdc42D(k_2 Bem1GEF_m + k_{2p} Bem1GEFCdc42T) + k_{2r}\left(GAP_c + \gamma GAP^*_c\right) Cdc42T$$

$$\frac{\partial Cdc42T}{\partial t} = D_m\nabla^2 Cdc42T + Cdc42D(k_2 Bem1GEF_m + k_{2p} Bem1GEFCdc42T) - k_{2r}\left(GAP_c + \gamma GAP^*_c\right) Cdc42T - (k_4 Bem1GEF_c + k_5 Bem1GEF_m) Cdc42T + (k_{4r} + k_{5r}) Bem1GEFCdc42T$$

$$\frac{\partial Bem1GEFCdc42T}{\partial t} = D_m\nabla^2 Bem1GEFCdc42T + (k_4 Bem1GEF_c + k_5 Bem1GEF_m) Cdc42T - (k_{4r} + k_{5r}) Bem1GEFCdc42T$$

$$\frac{\partial Bem1GEF_c}{\partial t} = D_c\nabla^2 Bem1GEF_c + \eta(-k_3 Bem1GEF_c + k_{3r} Bem1GEF_m - k_4 Bem1GEF_c \cdot Cdc42T + k_{4r} Bem1GEFCdc42T)$$

$$\frac{\partial Bem1GEF_m}{\partial t} = D_m\nabla^2 Bem1GEF_m + k_3 Bem1GEF_c - k_{3r} Bem1GEF_m - k_5 Bem1GEF_m \cdot Cdc42T + k_{5r} Bem1GEFCdc42T$$

$$\frac{\partial GAP_c}{\partial t} = D_c\nabla^2 GAP_c - \eta \cdot k_6 Bem1GEFCdc42T \cdot Cdc42T \cdot GAP_c + k_7 GAP^*_c$$

$$\frac{\partial GAP^*_c}{\partial t} = D_c\nabla^2 GAP^*_c + \eta \cdot k_6 Bem1GEFCdc42T \cdot Cdc42T \cdot GAP_c - k_7 GAP^*_c$$

(3) *Negative feedback via disruption of the Bem1p complex.* We assume that GTP-Cdc42p initiates a feedback loop that leads to the modification of the Bem1GEFCdc42T complex. Upon dissociation this yields Cdc42T and a modified Bem1GEF* that cannot re-bind Cdc42T until its modification has been reversed by a spatially uniform cytoplasmic process characterized by the first-order rate

constant k_7 (Figure S3). One possible mechanism for this negative feedback loop would be that the PAK Cla4p in one Bem1GEFCdc42T phosphorylates Bem1p complex components in a neighboring Bem1GEFCdc42T, changing their affinity for each other or for GTP-Cdc42p. In this scenario, the rate at which Bem1GEFCdc42T is modified is proportional to the square of the Bem1GEFCdc42T concentration. To keep additional assumptions to a minimum, we assumed that although the modified Bem1p complex cannot re-associate with GTP-Cdc42p, it retains basal GEF activity and transitions between the membrane and cytoplasm at the same rates as the unmodified complex. Model parameter values are listed in Table S3 below. This model is described by the following equations:

$$\frac{\partial Cdc42I_c}{\partial t} = D_c\nabla^2 Cdc42I_c + \eta(-k_1 Cdc42I_c + k_{1r} Cdc42D)$$

$$\frac{\partial Cdc42D}{\partial t} = D_m\nabla^2 Cdc42D + k_1 Cdc42I_c - k_{1r} Cdc42D - Cdc42D\left(k_2\left(Bem1GEF_m + Bem1GEF_m^*\right) + k_{2p}\left(Bem1GEFCdc42T + Bem1GEF^*Cdc42T\right)\right) + k_{2r} Cdc42T$$

$$\frac{\partial Cdc42T}{\partial t} = D_m\nabla^2 Cdc42T + Cdc42D\left(k_2\left(Bem1GEF_m + Bem1GEF_m^*\right) + k_{2p}\left(Bem1GEFCdc42T + Bem1GEF^*Cdc42T\right)\right) - k_{2r} Cdc42T - (k_4 Bem1GEF_c + k_5 Bem1GEF_m) Cdc42T + k_{5r} Bem1GEFCdc42T + k_{5r} Bem1GEF^*Cdc42T$$

$$\frac{\partial Bem1GEFCdc42T}{\partial t} = D_m\nabla^2 Bem1GEFCdc42T + (k_4 Bem1GEF_c + k_5 Bem1GEF_m) Cdc42T - k_{5r} Bem1GEFCdc42T - k_6 Bem1GEFCdc42T^2$$

$$\frac{\partial Bem1GEF^*Cdc42T}{\partial t} = D_m\nabla^2 Bem1GEF^*Cdc42T + k_6 Bem1GEFCdc42T^2 - k_{5r} Bem1GEF^*Cdc42T$$

$$\frac{\partial Bem1GEF_c}{\partial t} = D_c\nabla^2 Bem1GEF_c + \eta(-k_3 Bem1GEF_c + k_{3r} Bem1GEF_m - k_4 Bem1GEF_c \cdot Cdc42T) + k_7 Bem1GEF_c^*$$

$$\frac{\partial Bem1GEF_m}{\partial t} = D_m\nabla^2 Bem1GEF_m + k_3 Bem1GEF_c - k_{3r} Bem1GEF_m - k_5 Bem1GEF_m \cdot Cdc42T + k_{5r} Bem1GEFCdc42T$$

$$\frac{\partial Bem1GEF_m^*}{\partial t} = D_m\nabla^2 Bem1GEF_m^* + k_{5r} Bem1GEF^*Cdc42T - k_{3r} Bem1GEF_m^* + k_3 Bem1GEF_c^*$$

$$\frac{\partial Bem1GEF_c^*}{\partial t} = D_c\nabla^2 Bem1GEF_c^* + \eta\left(k_{3r} Bem1GEF_m^* - k_3 Bem1GEF_c^*\right) - k_7 Bem1GEF_c^*$$

Simulations with noise. All of the simulations results presented in the main text were deterministic. However, given the cell-to-cell variability of polarity dynamics observed experimentally, we expect that stochastic noise exerts significant influence on the dynamics. As a first step to see how minimal amounts of noise would affect the deterministic model, we added low-amplitude white noise to the Bem1p complex concentration at the membrane and in the cytoplasm (to preserve mass) and kept other species unaffected by noise. Our rationale for choosing these two species is that the cytoplasmic Bem1p complex is the least abundant species, thus fluctuations arising from stochastic variations in this complexes binding and release from the membrane are expected to be relatively large. We replaced the deterministic equations for $Bem1GEF_c$ and $Bem1GEF_m$ with:

$$\frac{\partial Bem1GEF_c}{\partial t} = D_c\nabla^2 Bem1GEF_c + \eta(-k_3 Bem1GEF_c + k_{3r} Bem1GEF_m - k_4 Bem1GEF_c \cdot Cdc42T) + k_7 Bem1GEF_c^* + \eta\sqrt{s}\xi(t)$$

$$\frac{\partial Bem1GEF_m}{\partial t} = D_m\nabla^2 Bem1GEF_m + k_3 Bem1GEF_c - k_{3r} Bem1GEF_m - k_5 Bem1GEF_m \cdot Cdc42T + k_{5r} Bem1GEFCdc42T - \sqrt{s}\xi(t)$$

where $\xi(t)$ is a Gaussian white noise term with strength $s = 0.0001$.

In the presence of this added noise with appropriate parameter values, the model predicts sustained oscillatory clusters as well as repeated competing and relocating clusters (Figure S3C). These simulations demonstrate that when stochastic effects are considered, the model can reproduce all the observed behavior with a single set of parameter values.

Parameter values. Model parameter values for all models are listed Table S3. Here we provide a brief description of how the model 1 parameter values were estimated.

The GDI-related rate constants (simplified to k1 and k1r in this work) were estimated based on real-time FRET measurements reporting interaction kinetics of recombinant human Cdc42p and GDI with insect cell membranes in vitro (Nomanbhoy et al., 1999).

The GEF- and GAP-regulated rate constants for GDP/GTP exchange and GTP hydrolysis by Cdc42p (k2, k2p, and k2r) were estimated based on in vitro rates of GDP release and GTP hydrolysis by recombinant yeast Cdc42p upon incubation with crude yeast lysates from synchronized cells (Howell et al., 2009).

Because we do not have specific data on the weak interaction of Bem1p complexes with the membrane, the relevant rate constants (k3 and k3r) were estimated based on similar PX-domain/membrane interactions in the literature (Goryachev and Pokhilko, 2008).

The binding/dissociation of the Bem1p complex to/from GTP-Cdc42p is a simplification of a more complex situation in which reversible binding reactions occur between GTP-Cdc42p and PAK, between PAK and Bem1p, and between Bem1p and Cdc24p. Because the SH3-mediated PAK-Bem1p interaction is likely to be the most labile of these, the relevant rate constants (k4, k5, and k5r) are estimated based on other SH3 interactions in the literature (Howell et al., 2009).

The membrane diffusion constant was estimated based on FRAP analysis of GFP-tagged prenylated reporters in latrunculin-treated cells (to eliminate endocytosis) (Marco et al., 2007).

Although the general ballpark values of these parameters are as realistic as we are able to estimate, the modeling results in this paper should be treated as qualitative rather than quantitative. Because the mechanism of negative feedback is unknown, the negative feedback parameters (k6 and k7) are purely speculative.

Bifurcation Diagram

We examined the dynamical behavior of models (1), (2) and (3) in the plane of total Cdc42p and Bem1p complex concentration. The range of concentration is chosen from 0 to 10-fold of the concentrations from previous studies (see Table S3 for 1x values: model 1).

There are 8 types of spatiotemporal behavior based on the number of fixed points and their stability with respect to spatial perturbations (two of them do not appear in the parameters used for Figure 4):

(i) Monostable: The spatially homogeneous steady state has only one fixed point and it is stable to all perturbations (white regions in all bifurcation diagrams: point 4, Figure S3B).

(ii) Bistable 1: Three spatially homogeneous fixed points exist, two of which are stable (blue regions in Figure 4D and G, Figure S3B). The fixed point with low GTP-Cdc42p is stable to all local perturbations, whereas the fixed point with high GTP-Cdc42p is stable to spatially homogenous perturbations but Turing unstable to spatial perturbations (point 1, Figure S3B).

(iii) Turing unstable: Only one fixed point exists, which is stable with regard to spatially uniform perturbations, but unstable given any small spatial perturbation (red regions in all bifurcation diagrams: points 2, 8, and 9, Figure S3). In this region away from the lower boundary, all models produce stable polarity site(s), which do not oscillate. The majority of polarization occurs in this region.

At the lower boundary of this region, close to the region with mixed Turing and Hopf instability (see below), models (2) and (3) show damped oscillatory polarization (point 8, Figure S3C). This type of behavior does not occur in model 1, and occurs in a relatively narrow region of parameter space for models 2 and 3.

(iv) Subcritical Turing unstable: For this case, only one uniform stable fixed point exists. However, it becomes unstable under sufficiently large spatial perturbations (the gray regions in all bifurcation diagrams: point 3, Figure S3B) (Cross and Hohenberg, 1993; Rovinsky and Menzinger, 1992).

(v) Excitable: Three spatially homogeneous fixed points exist, but only one is stable. The stable fixed point is an unstable spiral: large enough homogenous perturbations can excite transient homogeneous increases in the level of active Cdc42p (cyan regions in Figure 4E-G and Figure S3C). Spatially localized perturbations can induce transient polarization (point 5, Figure S3C) (Hecht et al., 2010; Xiong et al., 2010). Excitable behavior does not occur in model 1.

(vi) Turing and Hopf unstable: Only one fixed point exists, which is Hopf unstable and Turing unstable (green regions in Figure 4E-G and Figure S3C) (De Wit et al., 1996). This type of behavior does not occur in model 1.

In this region, the typical dynamics is alternating polarization and several rounds of uniform oscillation (points 6 and 7, Figure S3C). A spatially localized perturbation initiates formation of a polarized distribution of GTP-Cdc42p. Negative feedback then destabilizes polarization. As GTP-Cdc42p levels fall, the negative feedback is reduced, but remains sufficient to repress polarization. Thus, GTP-Cdc42p increases uniformly and then oscillates. After several such oscillations, the strength of negative feedback drops below threshold, enabling the positive feedback to accumulate GTP-Cdc42 locally. During polarization of GTP-Cdc42, the negative feedback increases again, starting another round of uniform oscillations. However, noise converts the uniform oscillations to oscillatory clustering and induces relocation and competition between multiple clusters.

Using appropriate parameter values, there are two other types of behavior:

(vii) Bistable 0: Three fixed points exist for spatially homogeneous concentrations, two of which are stable with different levels of active Cdc42p. Both fixed points are stable to spatial perturbations.

(viii) Hopf unstable: Only one fixed point exists that is unstable to all perturbations. The long-term behavior of the system is uniform oscillations of active Cdc42p.

The stability of (i), (ii), (iii), (v), (vii) and (viii) were assessed by numerically determining the steady state and calculating the eigenvalues for the linearized reaction equations in 1D. The Turing instability in (iii) and (vi) was determined by linear stability analysis

(Murray, 2003). The boundary of region (iv) was determined by numerical simulations. All three models show similar behaviors in planes of other parameter values.

Competition and Equalization of Two Polarity Foci

We used model 1 (positive feedback only) and model 3 (with negative feedback) to examine how negative feedback affects competition between polarized foci. Simulations were done on a 1D line (L = 5π μm) with periodic boundary conditions, representing a cell perimeter.

To simulate competition between two unequal GTP-Cdc42p foci, we evolved a symmetric two-peak solution for the points in parameter space shown in Figure 6. This was done by transiently including a spatial dependence of the rate constant k_3 for Bem1 binding to the membrane. Specifically, we took $k_3(\theta)$ to consist of two identical Gaussian distributions centered at $\pi/2$ and $3\pi/2$. After the spatial dependence of k_3 was removed and the two peaks had reached steady state, we adjusted the profile of GTP-Cdc42p from a 50:50 ratio between the peaks to various other ratios (55:45, 60:40, 70:30, 80:20 or 90:10) keeping total Cdc42p constant. The shared points (white circles in Figure 6) are limited to low Bem1p complex concentrations because model 1 could not sustain a two-peak distribution with larger amounts of Bem1p complex: once the spatial dependence of k_3 was withdrawn, the peaks flattened out to a homogeneous distribution that was unstable to spatial perturbation.

The competition simulations for each point started with the two-peak profiles adjusted as described above. We defined the duration of competition as the time taken to reach a state in which the peak GTP-Cdc42p concentration in the larger focus was 10-fold that of the smaller focus.

Whereas all points tested for model 1 (positive feedback only) displayed competition, in model 3 (with negative feedback) there was a transition from competition (point #1, Figure S5) to conditional equalization (point #2, Figure S5) as the total amounts of Cdc42p and the Bem1p complex were increased. By conditional equalization we mean that the two peaks became equal in size if the initial difference was less than a certain threshold. As the total Cdc42p and Bem1p complex amounts were increased further, two different peaks would equalize regardless of their relative size (Figure 6E; point #3, Figure S5). These three behaviors are depicted as blue (competition), green (equalization), and blue-green (conditional equalization) regions in Figure S5, as determined by sampling 53 randomly distributed points.

To examine how this behavior impacts a biologically realistic situation, we asked how many peaks would form if simulations were initiated with a variety of initial conditions. We show three representative points in Figure S5C. In the competition region, only one peak formed no matter what initial conditions were used (point #1, Figure S5C). In the conditional equalization region, different initial conditions led to either one or two peaks (point #2, Figure S5C). In the equalization region, two peaks of GTP-Cdc42p were established independent of the initial conditions (point #3, Figure S5C).

SUPPLEMENTAL REFERENCES

Baudin, A., Ozier-Kalogeropoulos, O., Denouel, A., Lacroute, F., and Cullin, C. (1993). A simple and efficient method for direct gene deletion in *Saccharomyces cerevisiae.* Nucleic Acids Res. *21*, 3329–3330.

Bi, E., Chiavetta, J.B., Chen, H., Chen, G.C., Chan, C.S., and Pringle, J.R. (2000). Identification of novel, evolutionarily conserved Cdc42p-interacting proteins and of redundant pathways linking Cdc24p and Cdc42p to actin polarization in yeast. Mol. Biol. Cell *11*, 773–793.

Bose, I., Irazoqui, J.E., Moskow, J.J., Bardes, E.S., Zyla, T.R., and Lew, D.J. (2001). Assembly of scaffold-mediated complexes containing Cdc42p, the exchange factor Cdc24p, and the effector Cla4p required for cell cycle-regulated phosphorylation of Cdc24p. J. Biol. Chem. *276*, 7176–7186.

Cross, M.C., and Hohenberg, P.C. (1993). Pattern formation outside of equilibrium. Rev. Mod. Phys. *65*, 851–1112.

De Wit, A., Lima, D., Dewel, G., Borckmans, P., and Borckmans, P. (1996). Spatiotemporal dynamics near a codimension-two point. Phys. Rev. E Stat. Phys. Plasmas Fluids Relat. Interdiscip. Topics *54*, 261–271.

Goryachev, A.B., and Pokhilko, A.V. (2008). Dynamics of Cdc42 network embodies a Turing-type mechanism of yeast cell polarity. FEBS Lett. *582*, 1437–1443.

Gulli, M.P., Jaquenoud, M., Shimada, Y., Niederhäuser, G., Wiget, P., and Peter, M. (2000). Phosphorylation of the Cdc42 exchange factor Cdc24 by the PAK-like kinase Cla4 may regulate polarized growth in yeast. Mol. Cell *6*, 1155–1167.

Hecht, I., Kessler, D.A., and Levine, H. (2010). Transient localized patterns in noise-driven reaction-diffusion systems. Phys. Rev. Lett. *104*, 158301.

Howell, A.S., Savage, N.S., Johnson, S.A., Bose, I., Wagner, A.W., Zyla, T.R., Nijhout, H.F., Reed, M.C., Goryachev, A.B., and Lew, D.J. (2009). Singularity in polarization: rewiring yeast cells to make two buds. Cell *139*, 731–743.

Johnson, J.L., Erickson, J.W., and Cerione, R.A. (2009). New insights into how the Rho guanine nucleotide dissociation inhibitor regulates the interaction of Cdc42 with membranes. J. Biol. Chem. *284*, 23860–23871.

Keaton, M.A., Szkotnicki, L., Marquitz, A.R., Harrison, J., Zyla, T.R., and Lew, D.J. (2008). Nucleocytoplasmic trafficking of G2/M regulators in yeast. Mol. Biol. Cell *19*, 4006–4018.

Kozubowski, L., Saito, K., Johnson, J.M., Howell, A.S., Zyla, T.R., and Lew, D.J. (2008). Symmetry-breaking polarization driven by a Cdc42p GEF-PAK complex. Curr. Biol. *18*, 1719–1726.

Longtine, M.S., McKenzie, A., III, Demarini, D.J., Shah, N.G., Wach, A., Brachat, A., Philippsen, P., and Pringle, J.R. (1998). Additional modules for versatile and economical PCR-based gene deletion and modification in *Saccharomyces cerevisiae.* Yeast *14*, 953–961.

Marco, E., Wedlich-Soldner, R., Li, R., Altschuler, S.J., and Wu, L.F. (2007). Endocytosis optimizes the dynamic localization of membrane proteins that regulate cortical polarity. Cell *129*, 411–422.

Murray, J.D. (2003). Mathematical Biology II: Spatial Models and Biomedical Applications (New York: Springer).

Nomanbhoy, T.K., Erickson, J.W., and Cerione, R.A. (1999). Kinetics of Cdc42 membrane extraction by Rho-GDI monitored by real-time fluorescence resonance energy transfer. Biochemistry *38*, 1744–1750.

Rovinsky, A., and Menzinger, M. (1992). Interaction of Turing and Hopf bifurcations in chemical systems. Phys. Rev. A *46*, 6315–6322.

Schenkman, L.R., Caruso, C., Pagé, N., and Pringle, J.R. (2002). The role of cell cycle-regulated expression in the localization of spatial landmark proteins in yeast. J. Cell Biol. *156*, 829–841.

Sikorski, R.S., and Hieter, P. (1989). A system of shuttle vectors and yeast host strains designed for efficient manipulation of DNA in *Saccharomyces cerevisiae.* Genetics *122*, 19–27.

Slaughter, B.D., Das, A., Schwartz, J.W., Rubinstein, B., and Li, R. (2009). Dual modes of cdc42 recycling fine-tune polarized morphogenesis. Dev. Cell *17*, 823–835.

Takahashi, S., and Pryciak, P.M. (2008). Membrane localization of scaffold proteins promotes graded signaling in the yeast MAP kinase cascade. Curr. Biol. *18*, 1184–1191.

Tong, Z., Gao, X.D., Howell, A.S., Bose, I., Lew, D.J., and Bi, E. (2007). Adjacent positioning of cellular structures enabled by a Cdc42 GTPase-activating protein-mediated zone of inhibition. J. Cell Biol. *179*, 1375–1384.

Wedlich-Soldner, R., Altschuler, S., Wu, L., and Li, R. (2003). Spontaneous cell polarization through actomyosin-based delivery of the Cdc42 GTPase. Science *299*, 1231–1235.

Wedlich-Soldner, R., Wai, S.C., Schmidt, T., and Li, R. (2004). Robust cell polarity is a dynamic state established by coupling transport and GTPase signaling. J. Cell Biol. *166*, 889–900.

Wu, H., and Brennwald, P. (2010). The function of two Rho family GTPases is determined by distinct patterns of cell surface localization. Mol. Cell. Biol. *30*, 5207–5217.

Xiong, Y., Huang, C.H., Iglesias, P.A., and Devreotes, P.N. (2010). Cells navigate with a local-excitation, global-inhibition-biased excitable network. Proc. Natl. Acad. Sci. USA *107*, 17079–17086.

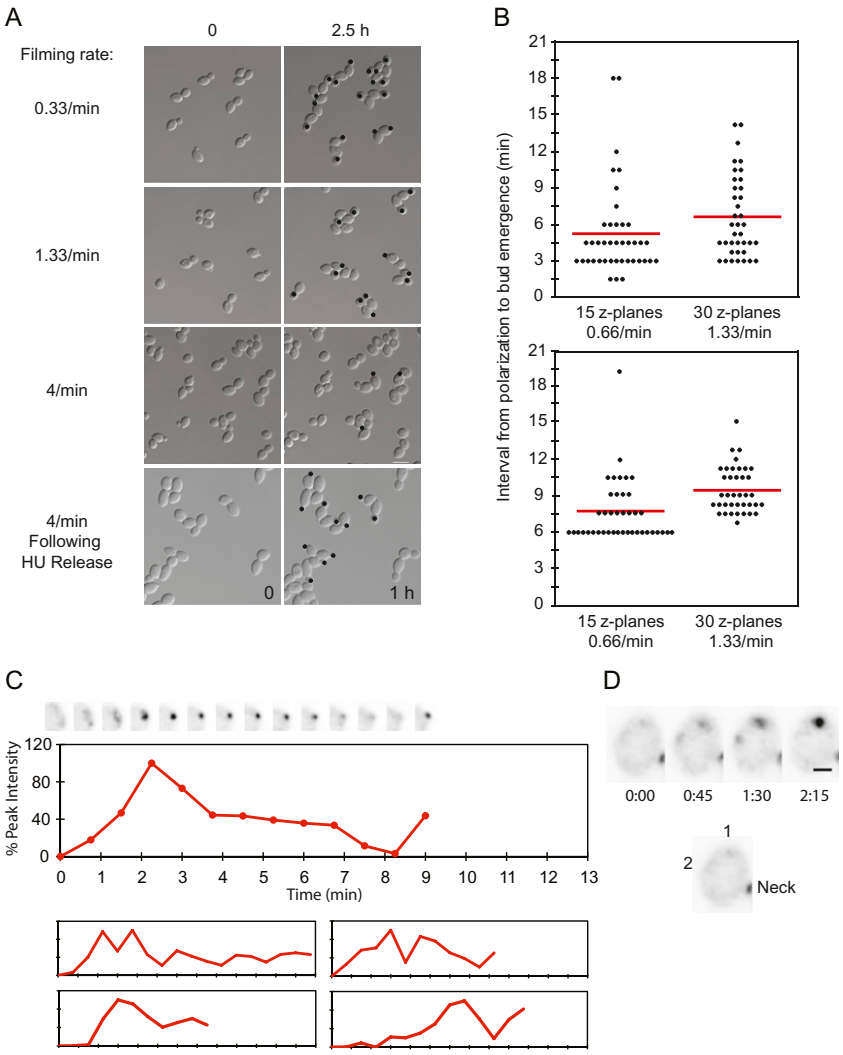

Figure S1. Synchronization with HU Reduces Phototoxicity, Allowing Faster Filming with Minimal Perturbation, Related to Figure 1

(A) Movies of yeast cells (DLY9201) with 15 Z-plane exposures (GFP and DIC illumination) were taken at the indicated time lapse rates. The top six panels show DIC images of fields of cells at the start (left) and after 2.5 hr of imaging (right). Black dots indicate successful budding events occurring during the filming interval. Increasing the frequency of illumination clearly delays or blocks budding. The bottom panels show a similar experiment at high filming rate for cells that were first arrested and then released from HU arrest prior to filming as described in experimental procedures. Multiple budding events occurred during the first 1 hr of filming (bottom right), and these cells went on to bud a second time after completing the cell cycle (not shown). Thus, pretreatment with HU rendered the cells more light-resistant. We speculate that the stress responses triggered by HU provide cross-protection against phototoxicity.

(B) Comparison of polarization and budding kinetics in cells released from HU arrest and filmed using previous non-perturbing but lower-resolution (15 Z-planes every 90 s) or higher-resolution (30 Z-planes every 45 s) conditions. Top: each symbol represents one *BEM1-GFP/BEM1-GFP rsr1*Δ*/rsr1*Δ (DLY9200) cell, and reports the interval from when Bem1p-GFP first concentrated at the neck (cytokinesis) to when a new polarity cluster was first detected. The range of intervals is similar in both filming conditions, though comparison of the average intervals (red lines) suggests that more frequent filming did marginally delay polarization. Bottom: similar plot showing interval from polarity cluster formation to bud emergence. Here it seems likely that the slightly longer interval reported in the higher-resolution movies stems from more accurate estimation of when cells first polarize.

(C) Polarization dynamics in asynchronous *BEM1-GFP/BEM1-GFP rsr1*Δ*/rsr1*Δ cells breaking symmetry. Inverted images (so dark spots represent concentrations of Bem1p-GFP) are shown. Without HU pre-treatment, high-resolution filming becomes phototoxic (see above). Here we document cells that happened to polarize in the first ~30 min of filming, hoping to limit phototoxic effects. Top: Cropped images of the polarization site at 45 s intervals: t = 0 is 45 s before the first detection of polarized signal, and trace ends at bud emergence. Middle: Amount of Bem1p-GFP in the cluster. Bottom: 4 other cells. The major difference with HU-synchronized cells (Figure 1) is that initial clustering of Bem1p-GFP is slower, and in some cells there is a period of faint polarity prior to growth of the cluster. We speculate that G1 cyclin/CDK activity (which triggers polarization (Gulli et al., 2000)) may ramp up more slowly in unsynchronized cells than in HU-synchronized cells, which are much larger. The dynamics of CDK activation may impact the initial growth of the cluster.

(D) Growth of multiple Bem1p clusters (numbered in the key at right) and resolution to a single cluster in asynchronous *BEM1-GFP/BEM1-GFP rsr1*Δ*/rsr1*Δ cell breaking symmetry.

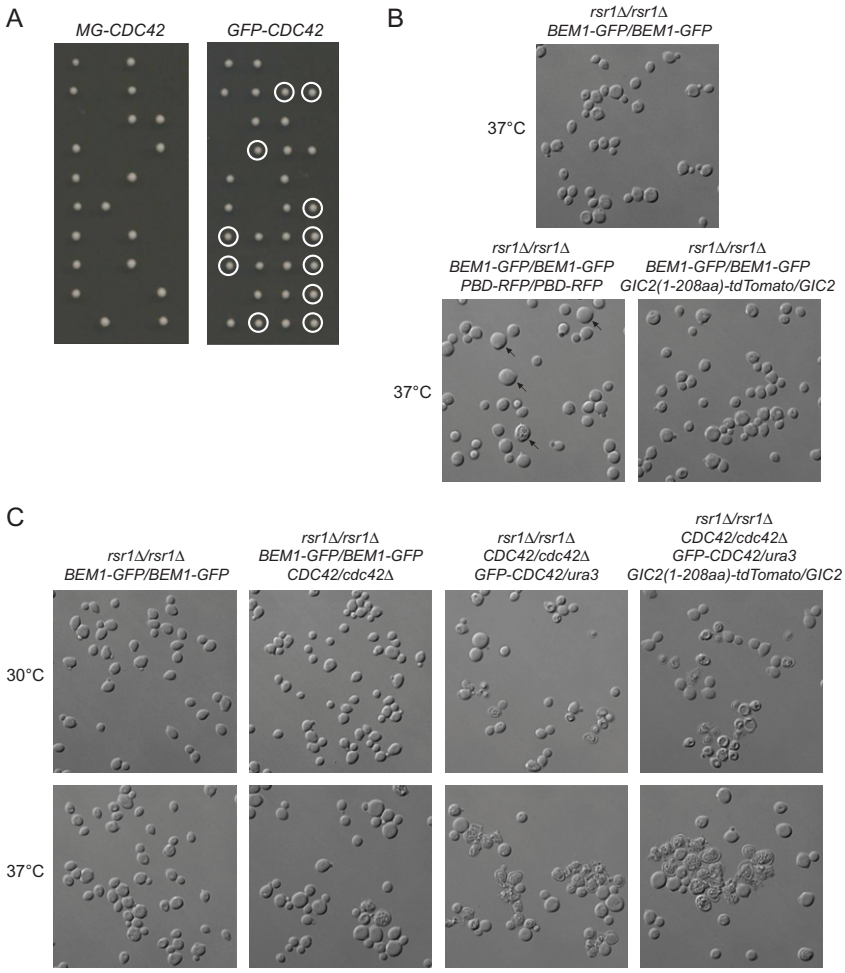

Figure S2. Functionality and Toxic Effects of Expressing Probes to Detect Cdc42p Localization, Related to Figure 2

(A) MG-CDC42 and GFP-CDC42 probes are not fully functional. Most published data on Cdc42p localization were obtained using the myc-GFP-Cdc42p (MG-CDC42) probe (Slaughter et al., 2009; Wedlich-Soldner et al., 2004), but those studies expressed the probe in addition to endogenous Cdc42p. To assess whether or not that probe is functional, we integrated a single copy into the genome of a diploid cell (DLY12831: the probe was expressed at comparable levels to endogenous Cdc42p and the GFP localization was as previously reported), deleted one copy of endogenous *CDC42*, and sporulated and dissected the diploid. As shown in the left panel, the tetrads (4 spores in a row) exhibited 2:2 segregation for viability at room temperature, and markers indicated that all *cdc42*Δ spores failed to form colonies regardless of whether or not they contained the MG-CDC42 probe. Thus, at least in our strain background, this probe is not functional at endogenous levels of expression. We therefore tested a different GFP-Cdc42p probe, which was reported to complement *cdc42*Δ mutants in a temperature-sensitive manner (Bi et al., 2000). Consistent with that report, upon sporulation of a heterozygous diploid (DLY12833) we readily obtained viable *cdc42*Δ GFP-Cdc42p spore colonies at room temperature (circled in right panel). Because we filmed cells at 30°C, where this probe is unable to complement Cdc42p function, we used heterozygous diploids containing one copy of endogenous *CDC42* and one copy of *GFP-CDC42*. We note that the lack of a fully functional probe for Cdc42p localization reduces confidence in the validity of this and all other published live-cell studies of Cdc42p localization.

(B) The PBD-RFP (GTP-Cdc42p-binding) probe is somewhat toxic. A probe to specifically detect GTP-Cdc42p has been developed based on a fragment of the Cdc42p effector Gic2p that contains a CRIB (Cdc42/Rac interactive binding) domain fused to tdTomato (Tong et al., 2007). Homozygous expression of this probe integrated at the *URA3* locus led to the appearance of large cells and lysed cells (arrows), especially at elevated temperature. Panels show DIC images of fields of cells grown to mid-log phase in synthetic media at 37°C. To reduce toxicity, we generated a heterozygous version of the same probe at the endogenous *GIC2* locus, which is expressed at lower levels. This probe reduced but did not eliminate the incidence of misshapen or lysed cells. Strains are DLY9200, DLY9889, and DLY13157.

(C) The GFP-Cdc42p probe causes mild dominant toxicity, especially in combination with the PBD-RFP probe. Images of cells grown as in B, showing (left to right) controls (DLY9200), rare incidence of large and lysed cells in *CDC42*/*cdc42*Δ diploid heterozygotes (DLY13824), stronger defects in *CDC42*/*cdc42*Δ diploids expressing one copy of GFP-Cdc42p (DLY13859), and strongest defects in *CDC42*/*cdc42*Δ diploids expressing one copy of GFP-Cdc42p and one copy of PBD-RFP (DLY13164).

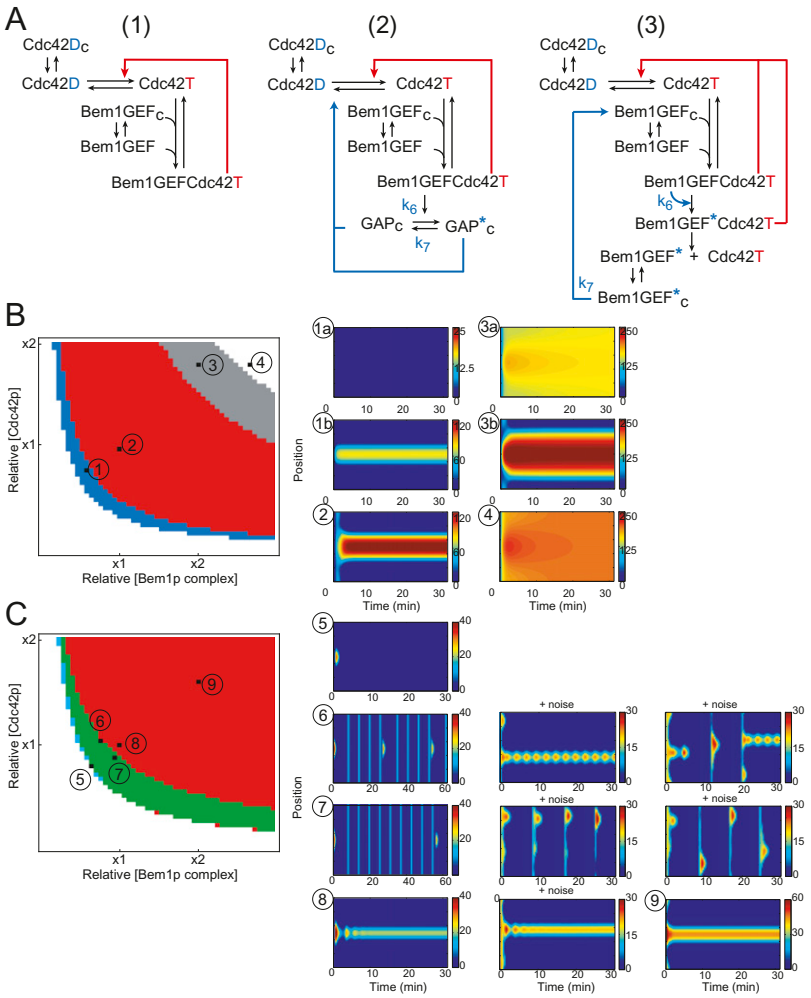

Figure S3. Models with and without Negative Feedback and Spatiotemporal Dynamics in Different Parts of Model Parameter Space

(A) Model 1 has positive feedback only, model 2 has a negative feedback loop via activation of a cytoplasmic GAP, and model 3 has negative feedback via disruption of the Bem1p complex. The reaction schemes correspond to the cartoons diagrammed in Figure 4A. See text for details. Bifurcation diagrams (B-C) are color-coded as in Figure 4. Simulations depict the evolution of GTP-Cdc42p concentration (color) along the cell perimeter (*y* axis) with time (*x* axis). At the start of the simulation, the system is in the low GTP-Cdc42p steady state and a small perturbation is applied to the center of the perimeter.

(B) Behaviors of Model 1. Left: expanded view of the lower-left quadrant of the [Cdc42]-[Bem1 complex] bifurcation diagram: numbered symbols indicate positions simulated at right. (#1) Bistable 1: depending on the strength of the perturbation, an initial perturbation decays back to the uniform steady state (1a) or grows to reach a polarized steady state (1b). [Cdc42] = 4 μM, [Bem1-complex] = 0.01 μM. (#2) Turing Unstable: a small perturbation always develops to a polarized state. [Cdc42] = 5 μM, [Bem1-complex] = 0.017 μM. (#3) Subcritical Turing Unstable: depending on the strength of the perturbation, an initial perturbation decays to a uniform steady state (3a) or grows to reach a polarized steady state (3b). [Cdc42] = 9 μM, [Bem1-complex] = 0.034 μM. (#4) Monostable: any initial perturbation leads to a uniform steady state. [Cdc42] = 9 μM, [Bem1-complex] = 0.045 μM.

(C) Behaviors of Model 3. Left: expanded view of the lower-left quadrant of the [Cdc42]-[Bem1 complex] bifurcation diagram: numbered symbols indicate positions simulated at right. (#5) Excitable: a perturbation initially grows but then decays back to the uniform steady state. [Cdc42] = 4 μM, [Bem1-complex] = 0.011 μM. (#6) Mixed Turing and Hopf Unstable: an initial perturbation leads to sustained oscillations, switching between uniform and localized patterns. [Cdc42] = 5.2 μM, [Bem1-complex] = 0.0135 μM. (#7) Mixed Turing and Hopf Unstable (closer to the center of the region): similar to (#6), but less frequent localized patterns are interspersed with more frequent spatially uniform oscillations. [Cdc42] = 4.4 μM, [Bem1-complex] = 0.016 μM. (#8) Turing Unstable (close to Hopf-Turing unstable region): an initial perturbation leads to damped oscillation on the way to a polarized steady state. [Cdc42] = 5 μM, [Bem1-complex] = 0.01775 μM. (#9) Turing Unstable (far from Hopf-Turing unstable region): a small perturbation develops to a polarized state with little oscillation. [Cdc42] = 8 μM, [Bem1-complex] = 0.034 μM. Although not depicted, simulations in the Subcritical Turing Unstable (gray) and Monostable (white) regions of Model 3 behave similarly to the corresponding regions of Model 1.

For points #6-8, we also show simulations with added noise (indicated by "+noise"), which alters polarity factor dynamics (see Supplemental Text for details). The middle and right columns of the first two rows represent two realizations of the stochastic process. In the presence of noise, simulations in the region with both Hopf and Turing instability (points #6 and #7) can exhibit sustained oscillatory clustering (first two rows, middle panels) and simulations in the Turing only region (point #8) were more susceptible to damped oscillations (bottom row, middle panel). Stochastic effects also generated competing (Top row, right panel, times > 20 min) and relocating clusters (first two rows, right panels). Because the simulations are stochastic, "sustained" oscillations can eventually be destroyed and new clusters emerge in different locations.

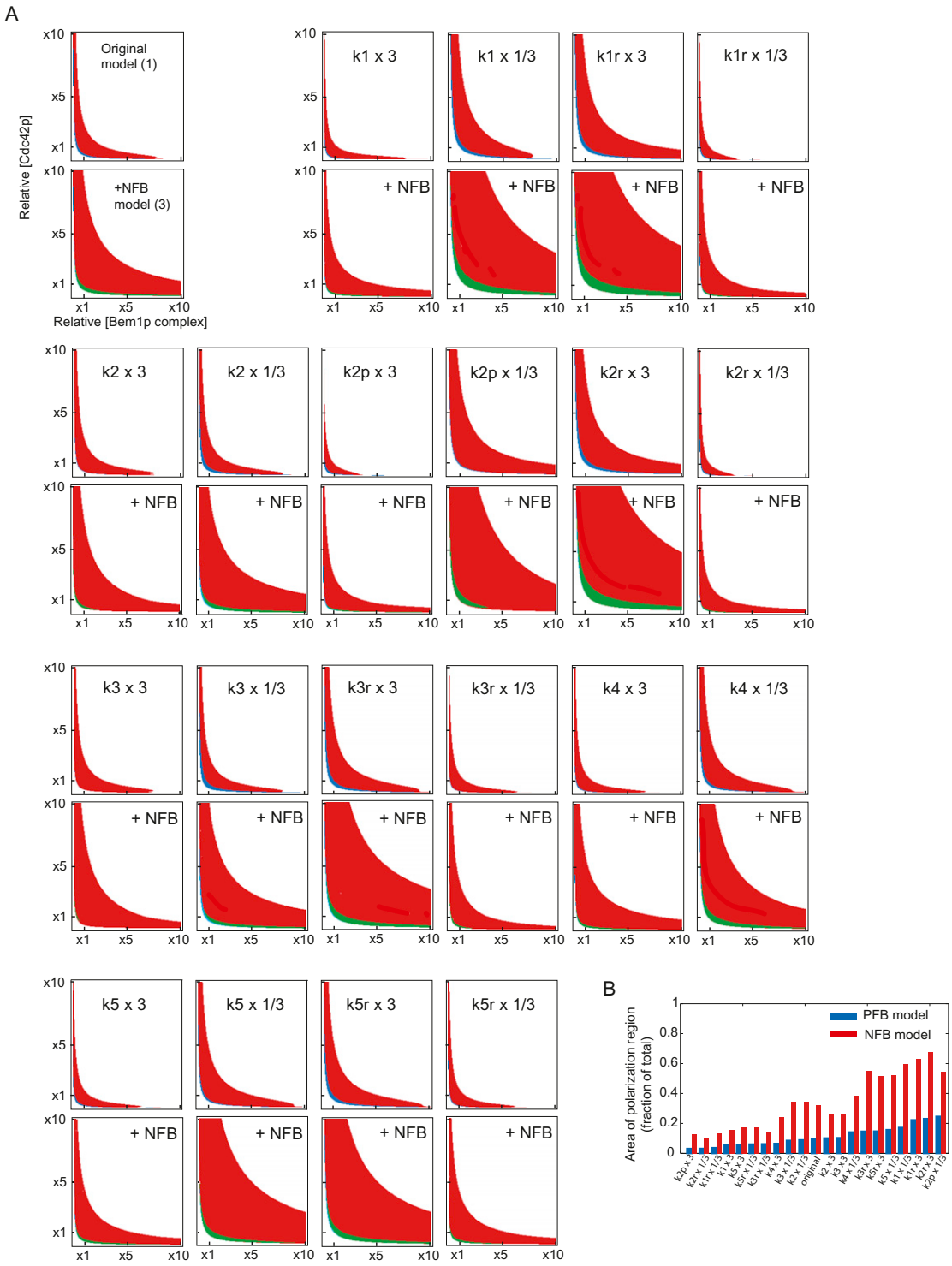

Figure S4. The Effect of Negative Feedback on Robustness Does Not Depend on Specific Rate Parameters, Related to Figure 4

(A) Bifurcation diagrams of model 1 (positive feedback only) and model 3 (with negative feedback via the Bem1p complex) are displayed as pairs (model 1 above, model 3 below) for various values of the rate constants. Each parameter was increased or decreased 3-fold from its original value, and the Turing-unstable region (red) was determined by linear stability analysis.

(B) Summary indicating that negative feedback increases the polarization region in all cases. The area of the polarization region (red) as a fraction of the total area in relative Cdc42p and Bem1p complex space is plotted as a measure of the model's robustness to varying levels of polarity factors. Blue and red bars report model 1 and 3 respectively. Paired bars use the same parameter set, and pairs are ordered by increasing robustness of model 1.

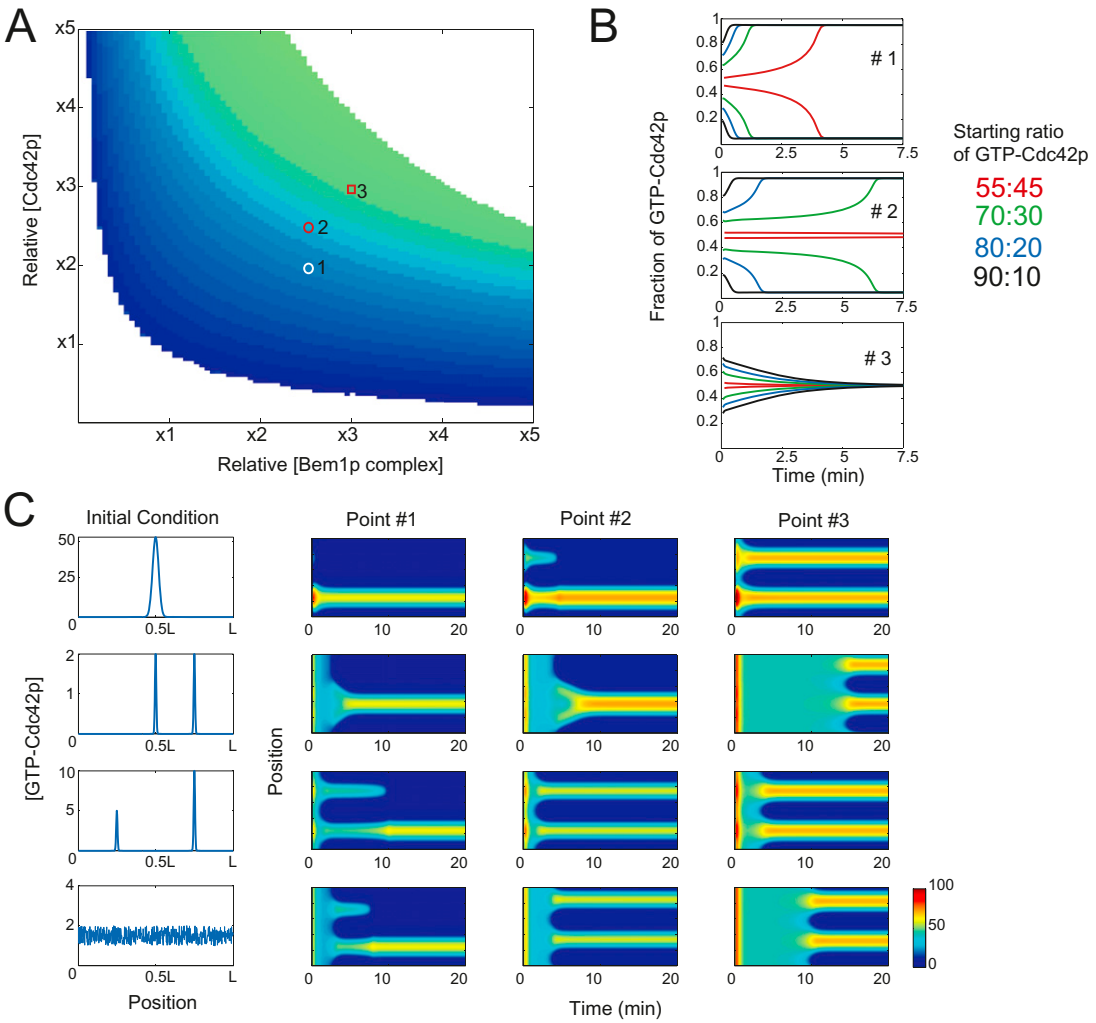

Figure S5. Competition and Equalization between Clusters in Model 3, Related to Figure 6

(A) Three regions with different types of competition behavior in [Cdc42]-[Bem1-complex] bifurcation diagram of Model 3. Blue region (competition): two unequal peaks compete and the larger one wins. Green region (equalization): two unequal peaks equalize and then coexist. Blue-green region (conditional equalization): competition or equalization, depending on the starting difference between the two peaks (see B). White region: no polarization occurs. The numbered symbols indicate positions simulated in B.

(B) Simulated competition and equalization. Simulations were initiated with two peaks at opposite ends of the cell perimeter, containing the indicated color-coded ratios of GTP-Cdc42p. The fraction of GTP-Cdc42p in each peak is plotted as a function of time. Top: at point #1 (white circle), the two peaks always compete. Middle: at point #2 (red circle), two similar-sized peaks equalize (e.g., ratio 55:45) but very unequal peaks compete (e.g., ratio 70:30). Bottom: at point #3 (red square), two peaks always equalize.

(C) Simulated behavior with different initial conditions. Simulations were initiated with the initial perturbations in GTP-Cdc42p shown at left, at the points in the bifurcation diagram (#1-3) indicated in A. Top: a single initial spike leads to development of one peak at points #1 and #2, but two peaks at point #3. Second row: two nearby spikes merge to form a single peak at points #1 and #2, but two peaks at point #3. Third row: two unequal spikes compete at point #1 but equalize at points #2 and 3. Bottom: a noisy initial input develops to a single peak at point #1 but two equal peaks at points #2 and 3. Thus, in the competition region all simulations develop a single peak and in the equalization region all simulations develop two peaks, independent of initial conditions. In between, the number of peaks depends on initial condition (point #2).